Available online at www.sciencedirect.com
SCIENCE DIRECT
Journal of Physics and Chemistry of Solids 65 (2004) 1957–1966
JOURNAL OF PHYSICS AND CHEMISTRY OF SOLIDS
www.elsevier.com/locate/jpcs

Topological analysis of charge density in heptasulfur imide (S_7NH) from isolated molecule to solid

Chi-Rung Lee[b], Ting-Hua Tang[a], Likey Chen[a], Chih-Chieh Wang[c], Yu Wang[a,*]

[a]*Department of Chemistry, National Taiwan University, Taipei, Taiwan, ROC*
[b]*Department of Chemical Engineering, Minghsin University of Science and Technology, Hsin-Chu, Taiwan, ROC*
[c]*Department of Chemistry, Soochow University, Taipei, Taiwan, ROC*

Abstract

Intra and intermolecular interactions of heptasulfur imide (S_7NH) are investigated in terms of topological properties analyses, such analyses are applied to both experimental (multipole model) and theoretically calculated (DFT and PDFT calculations) charge densities of the isolated molecule and of the crystal. The same analyses are also applied to a multipole model density obtained from theoretically (PDFT) derived structural amplitudes. The covalent bond character of S–N, N–H and S–S bonds are well described in terms of density, ρ_b, and total energy density, H_b, at the bond critical point r_c, though it is clear that the S–S bonds are weaker shared interactions than those of N–H and S–N bonds. Lone pair electron regions of sulfur and nitrogen atoms are revealed as the local charge concentration site from the Laplacian of charge density. The even weaker intermolecular interactions are well characterized; these include the N–H···S hydrogen bonding, N···S binding interactions and S···S binding interactions. All these intermolecular binding interactions are closed-shell interactions. The Laplacian of charge density demonstrates a directional intermolecular binding interaction. The corresponding intermolecular binding energies are derived by MP2/6-311+G(d,p) calculations. Atomic graph of each atom of the molecule is described in detail by the vertices, edges and faces of the polyhedron around the nucleus to illustrate such directional interactions.

Keywords: C. Ab initio calculations; C. X-ray diffraction

1. Introduction

The studies of molecules containing sulfur–sulfur bonds have drawn extensive attention in the past 20 years [1–20] not only on the bonding features of S–S bond and the necessity for the inclusion of d-polarization functions for the sulfur atoms, but also for its important role in the protein folding. Some studies of experimental deformation density distribution reveal various density distribution on S–S bond, such that a double maximum was found along the S–S bond of S_8 molecule [1]; a maximum at the midpoint of the S–S bonds was observed on $Na_2S_2O_6\cdot 2H_2O$, $Na_2S_2O_6\cdot 2D_2O$ [S–S = 2.14 Å] and $MgS_2O_3\cdot 6H_2O$ [S–S = 2.02 Å] [2–3]. Several thiathiophthene derivatives were investigated, little density accumulation was detected in the deformation density distribution along the S–S bonds [S–S = 2.14–2.51 Å] [5–12]. The similar results were also reproduced from theoretical studies [13]. Molecular structures and chemical bonding were determined by ab initio calculations for several sulfur–nitrogen compounds [4,20] using the 'atoms in molecules' (AIM) approach [21]. In the light of AIM approach, experimental and theoretical studies of the charge density distribution of $[(CH_3)_2CS_2]_2$ [14], as well as many types of interactions in other sulfur containing compounds have been studied [14,19,20,22–23,25] in terms of local charge concentration and local charge depletion of a Lewis acid–base concept [21]. The S···S intermolecular interaction in L-cystine was analyzed [19] in the same approach. This general phenomenon has been well studied in many types of interaction, such as formation of hydrogen bonds [22], the directional interaction of Cl_2 [23], the packing of S_4N_4 in solid state [4,20], the binding interactions in van der Waals dimers and trimers [24], the metal ligand bond in metal

* Corresponding author. Tel.: +886 2 2363 8377; fax: +886 2 2363 6359.
E-mail address: wangyu@ntu.edu.tw (Y. Wang).

0022-3697/$ - see front matter © 2004 Elsevier Ltd. All rights reserved.
doi:10.1016/j.jpcs.2004.08.007

complexes [25], the adsorption of molecules on surface [26] as well as the catalytic activities of some transition metal sulfides [27].

The Heptasulfur imide, S_7NH was studied by single crystal X-ray diffraction at 100 K and the electron density of the molecule was analyzed in terms of deformation density distribution [10]. It crystallized in an orthorhombic space group P_{nma}, $Z=4$, with cell parameters $a=7.842(2)$, $b=13.115(2)$, $c=7.6219(7)$ Å. The S_7NH molecule is in a crown shape structure, which is similar to that of cyclooctasulfur, S_8, with one sulfur atom replaced by an imide (NH) group. In order to extend our understanding of the nature of intramolecular S–N and S–S bonds as well as the intermolecular binding interactions between neighboring molecules of S_7NH in the solid state, the topological property analysis has been employed in the present study. The theoretical charge densities are obtained from DFT calculations for monomer and selected dimers. Additional calculation at the same level is made on S_8 molecule based on the experimental geometry [1] for the sake of valuable comparison. In addition, periodic density functional (PDFT) calculations for the electron density of the crystal have also been investigated. Taking advantage of the topological properties analyses, the comparison between experiment and theory is fully undertaken. Same approach was investigated on the thioures-S, S-dioxide [22(g)], where the intermolecular hydrogen bonds as well as the weak directional interactions were studied.

2. Computational details

2.1. Experimental data refinements

The experimental charge density was derived from the single crystal X-ray diffraction applying the multipole model (MM) [28]. The atomic electron density in MM is expression as follows

$$\rho_{at}(r) = P_c\rho_{core}(r) + P_v\kappa^3\rho_{valence}(\kappa r) + \sum_{l=0}^{l_{max}} \kappa'^3 R_l(\kappa' r) \sum_{m=0}^{l} P_{lm\pm} Y_{lm\pm}(\theta,\phi)$$

where the electron density is the sum of a spherical core electron part, $P_c\rho_{core}$, and a valence electron part. The valence part includes a spherical term, $P_v\kappa^3\rho_{valence}(r)$, and multipole parts in terms of spherical harmonics, $Y_{lm\pm}$. The coefficients of the multipole terms, $P_{lm\pm}$, P_v as well as the expansion–contraction κ, κ' are the parameters fitted through multipole refinement. Detailed description of the data collection and refinements as well as the deformation density distribution was given in the previous paper [10]. Multipole refinements were reinvestigated using the XD program [29]. The level of multipole expansion was extended up to quadrupole for hydrogen; up to octapole for nitrogen and up to hexadecapole for sulfur. The minimization function is based on F^2. During the refinement, H atom was moved along the N–H vector to make an N–H distance of 1.03 Å [30]. The n_l values ($l=1$–4) of S are set as 6, 6, 8, 8, where those of N are: 2, 2, 3 and of H are: 1, 2. The *kappa'*-restricted multipole model (KRMM) [31] was carried out at the final stage. With KRMM the radial κ' coefficients were fixed at values derived from multipole refinement of theoretically derived structure factors obtained from PDFT calculations (κ' coefficient for S1: 1.14; S2: 1.26; S3: 1.29; S4: 1.32 and N: 1.03). The ζ values of H, N, and S are 2.00, 3.84, and 3.95 $Å^{-1}$, respectively. The Laplacian distributions from experiment are depicted using XD program [29] and the contour maps of charge density distributions; iso-value surfaces of Laplacian distribution as well as bond paths are drawn by PROP program [32].

2.2. Molecular orbital calculations

All density functional theory (DFT) calculations including the monomer and the chosen dimers of heptasulfur imide were carried out using the GAUSSIAN 98 program [33]. The B3LYP functional [34,35] and basis set 6-311G(d,p) were used. In order to estimate the intermolecular binding energies, the MP2 calculations using 6-311+G(d,p) basis set were applied [36] including the correction for basis set superposition error (BSSE) [37]. Fully periodic density functional (PDFT) calculation on the crystal of the title compound with the comparable functional and basis set [B3LYP/6-311G(d,p)] was performed using CRYSTAL 98 [38]. The structural amplitudes were derived from this calculation. The multipole refinement [28] on these theoretically derived structural amplitudes was then applied (PDFT/MM). The κ' thus obtained were used for the experimental multipole model (KRMM).

2.3. Topological properties analysis of charge density distributions

Bond critical points (BCPs) and bond paths (BPs) of electron density can be used to construct a molecular graph. Since the BP is 'an universal indicator of bonded interactions' [39], the network of BPs therefore represents all atomic interactions in a given system. The electron density at BCP, ρ_b, is related to the bond strength or the bond order [40]. The sign of the Laplacian of density at the BCP, $\nabla^2\rho_b$, may be used to distinguish bonding type between the share interaction and the closed-shell interaction, however, exceptions do occur. It was suggested [40] that the total energy density value at the BCP, H_b, which is the sum of kinetic energy density G_b and potential energy density V_b, at the BCP, could be interpreted as the sufficient condition of a covalent bond when the sign of H_b is negative. Such value may be used as a measure for the covalency of a bond. The experimental H_b value is

estimated by a generalized approach of Abramov's expression [41,42]. The Laplacian distribution is a very useful tool, for the purpose of understanding the chemical reactivity and of revealing a directional interaction in the molecular crystal. The topological properties of Laplacian, $\nabla^2\rho(\mathbf{r})$, can be further quantified by its critical points, CPs. These CPs, construct the atomic graph around each atom. A correlation between these CPs of $\nabla^2\rho(\mathbf{r})$ in the valence shell and the location of the active site in molecule has been established [21,43]. In principle, a Lewis acid–base reaction occurs when a local density maximum (vertex) in the VSCC of the Lewis base aligns itself as far as possible with a local density minimum (face) in the VSCC of the Lewis acid. Starting at a BCP, paths for which the electron density decreases most rapidly are developed in all directions normal to the bond. The set of such paths defines a zero-flux surface separating a pair of bonded atoms. A set of these surfaces (one per bond) will partition a molecule into unique atom domains Ω. Numerical integration of the electron density within such a domain yields atomic AIM charge. The AIMPAC [44] and AIM98PC [45] programs were employed for the topological analyses of the charge density of monomer and dimer derived from DFT calculations. The TOPOND [46] program was employed for the PDFT crystal calculation.

3. Results and discussion

3.1. Multipole refinements

The molecular structure of heptasulfur imide with its atomic labeling and internal coordinates is shown in Fig. 1. The structural parameters are the same within SD as those given in the previous work [10]. The residual maps after the multipole refinements based on experimental structure amplitudes and the theoretically derived ones are displayed in Fig. 2a and b, respectively. In general the theoretical one shows little residual, the experimental one shows more noise (± 0.2 e Å^{-3}). The agreement indices

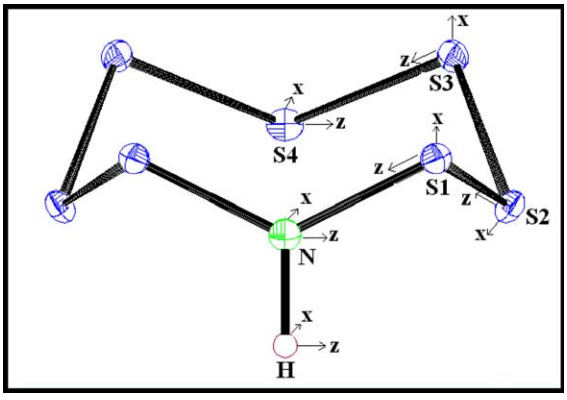

Fig. 1. The molecular structure of S_7NH with atomic labeling and the definition of internal coordinates.

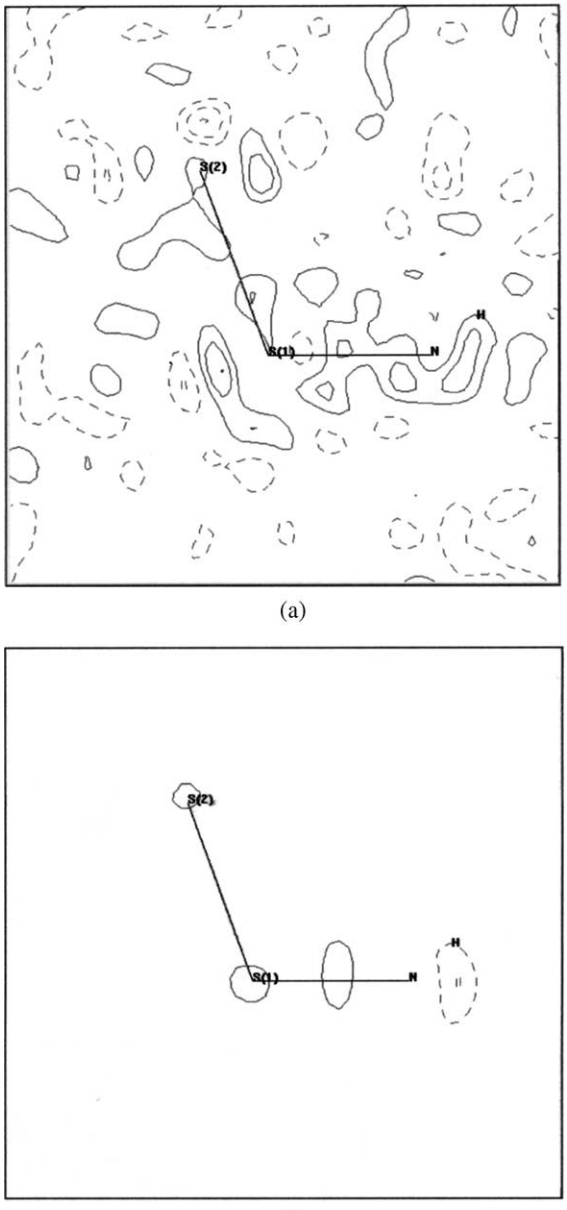

Fig. 2. The residual map of S_7NH based on (a) experimental structure factors (KRMM), (b) the theoretically derived structure factors (PDFT/MM). Contour interval: 0.1 e Å^{-3}, solid line, positive; dash line, negative.

of the multipole refinements are given in Table 1. The atomic parameters and the multipole coefficients from various refinements are qualitatively the same. Of course, the U_{ij}s are set to zero for the model density derived from PDFT calculation. The lists of multipole coefficients are in supplementary material. The additional parameters in the present study do improve the refinements. The refinement based on the theoretically derived *F*s is particularly successful with the lowest agreement indices. The κ' thus obtained for each atom is used for the subsequent density studies (KRMM).

Table 1
Agreement indices of various multipole refinements

	N_v	R_1[a]	R_{1w}[a]	R_2[a]	R_{2w}[a]	GOF[a]
MM [10]	145	0.0242	0.0194	0.0238	0.0268	1.82
MM	156	0.0182	0.0191	0.0226	0.0235	1.73
KRMM	151	0.0188	0.0193	0.0226	0.0348	1.76
PDFT/MM	126	0.0050	0.0054	0.0079	0.0108	1.69[b]

[a] $R_1 = \sum |F_o - F_c| / \sum F_o$; $R_{1w} = \left[\sum w|F_o - F_c|^2 / \sum wF_o^2\right]^{1/2}$; $R_2 = \sum |F_o^2 - F_c^2| / \sum F_o^2$; $R_{2w} = \left[\sum w|F_o^2 - F_c^2|^2 / \sum wF_o^4\right]^{1/2}$; GOF $= \left[\sum w|F_o - F_c|^2 / (NR - NV)\right]^{1/2}$ NR = 2874, NV, no. of variables.
[b] Refinement using unit weight.

3.2. Intramolecular bonding

The Laplacian of charge density distributions at three unique planes from calculated and from experimental results are depicted in Fig. 3. The local CCs around each atom at the plane are clearly observed in the Laplacian distributions. The shared-interaction characters along N–H, N–S and S–S are also manifested in these figures. All the essential features do reproduce in the experimental ones as in the theoretical ones. The ones using the theoretically derived *F*s imposed with the multipole model (PDFT/MM) show better agreement with the experiment (KRMM) than those from the purely calculated ones (PDFT). For example, the Laplacian distribution of S2–S3–S4 plane shown in Fig. 3e–h, indicate that the PDFT/MM one (Fig. 3h) agrees better with the KRMM one (Fig. 3f) than that of PDFT one (Fig. 3g).

Nine BCPs and one ring critical point in $\rho(\mathbf{r})$ are found both from experiment and from theory. The topological properties associated with the BCPs are tabulated in Table 2. In general, the ρ_b, $\nabla^2\rho_b$, and H_b values are in reasonable agreement between experiment and theory, taking the SD of 0.04 e Å^{-3} in experimental ρ_b value. The H–N, N–S and the S–S bonds are covalent having negative value of H_b and reasonable ρ_b values. According to the ρ_b and H_b values, N–H and N–S bonds are stronger than that of S–S bond. The S–S bond distances of the title compound are the same as those of S_8 [1] and L-cystine [19]. The theoretical ρ_b, $\nabla^2\rho_b$ and H_b values of these three compounds are quite consistent with one another (Table 2). Based on these values, one can conclude that the nature of chemical bond and the bond strength of these S–S bonds are quite close to that of S_8. However, the experimental ρ_b value of S3–S4 bond does appear different from other S–S bonds. A survey of the ρ_b values of S–S bonds in various compounds with S–S distances in the range of 2.00–2.51 Å is listed also in Table 2 for comparison. The ρ_b value is in the range of 0.37–1.14 e Å^{-3} and the corresponding S–S distance is in the range of 2.509–2.006 Å. The longer the S–S bond distance, the smaller is ρ_b. Unfortunately, we do not have many H_b values; only one is available for comparison in these compounds. The ρ_b values of H–N bond are weakened from isolated molecule (2.13 e Å^{-3}) to solid (1.88 e Å^{-3}). This might be due to the intermolecular binding interactions in crystal. Comparable findings are reported for O–H···O of KHC_2O_4 [47] and HCN [48]. Discrepancies in $\nabla^2\rho_b$ values of S–S bonds between the theory and experiment were discussed elsewhere [49]. The N–S bond length, 1.686 Å, is clearly shorter than the typical single bond (1.73 Å) [50] and the earlier study of charge density distribution [10] also indicated there is some 'π-character' of S–N bond. In the present theoretical calculations of the monomer and the crystal, the average value of ellipticity of this bond at BCP is $\varepsilon \cong 0.2$, which supports the π-character of S–N bond. The ρ_b value of 1.74 e Å^{-3} and the H_b value of -1.5 a.u. Å^{-3} also indicate a strong binding interaction. Moreover, based on the $\nabla^2\rho(r)$ distribution there are CCs about 0.4 Å above and below the N at the S1NS1′ plane. These CCs are well correlated with intermolecular interaction discussed in the following section.

3.3. Atom domains and atomic charge

The partitioning surfaces around each atom (atom domain) can be derived from the total electron density distribution. Atomic charges based on such partitioning both from the experiment and from theory are tabulated in Table 3. The atomic charges are such that the N–H group is carrying negative charge, S1 is positive charge, and the rest of S atoms are roughly neutral. There is a net charge transfer of ca. 1.2 e from two neighboring sulfur atoms and the hydrogen atom to the nitrogen atom in the theoretical calculation, which is similar to the calculated values of 1.22 and 1.29 e in the case of S_2N_2 and S_4N_4, respectively [4]. However, there is a net charge transfer of 1.5 e in experimental ones.

3.4. Atomic graphs of N and S atoms in monomer and in crystal

In general, the charge concentrations in the valence shell (VSCC) of an atom, as determined by the Laplacian of $\rho(\mathbf{r})$, are found to be in good agreement with the corresponding bonded and non-bonded pairs in Gillespie's VSEPR model of molecular geometry [51]. An atomic graph [21,45] is a polyhedron around the nucleus where the local density maxima in VSCC of the atom define the vertices, *V*. The unique pair of trajectories of the gradient of $\nabla^2\rho(\mathbf{r})$ that

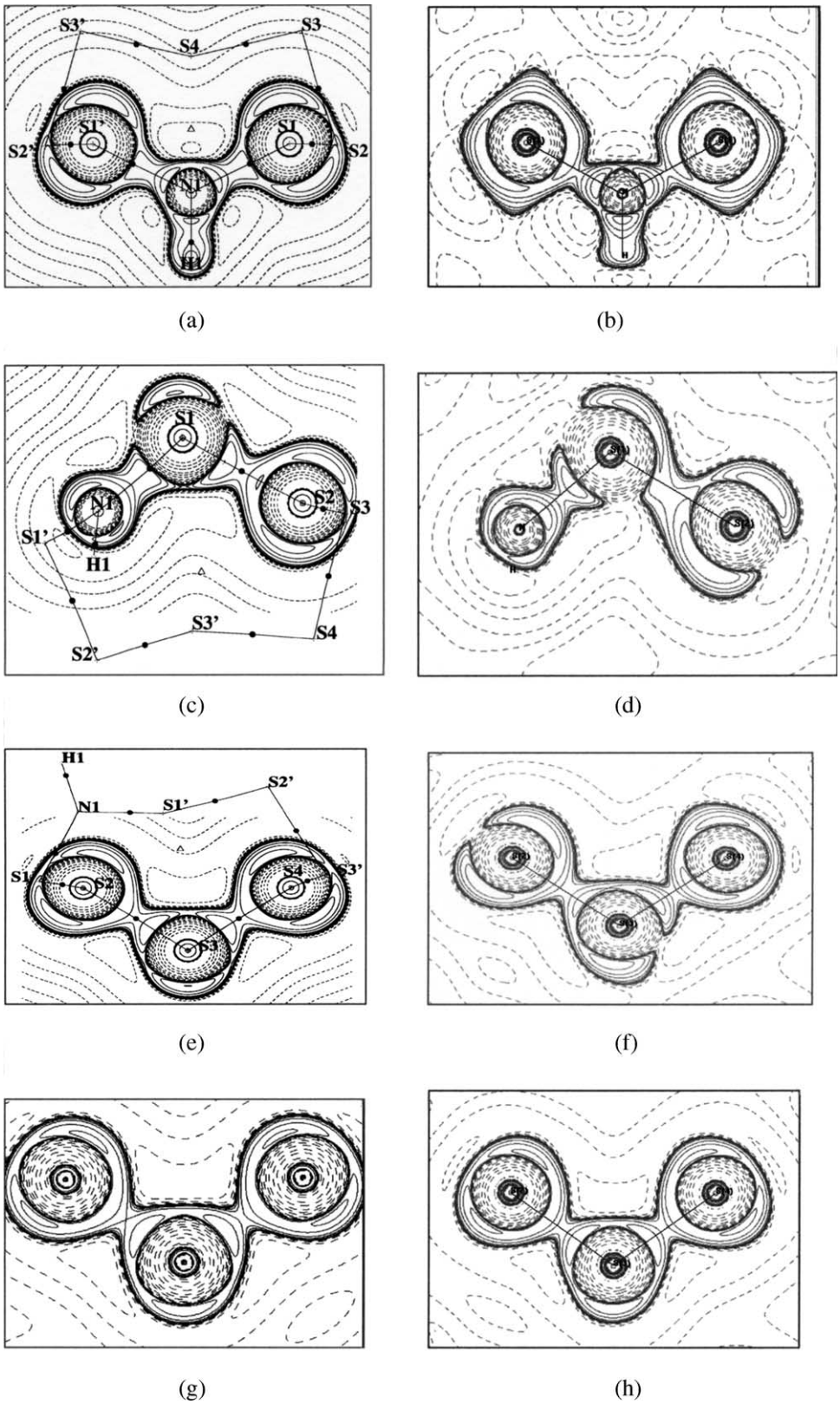

Fig. 3. The Laplacian distribution and the molecular graph of S_7NH at (a), (b) the S1–N1–S1′ plane; (c), (d) the N1–S1–S2 plane; (e)–(h) the S2–S3–S4 plane; (a), (c), (e) are from theory of isolated molecule and (b), (d), (f) are from experiment (KRMM), (g) is from PDFT calculation, (h) is from PDFT/MM. The heavy solid lines represent the BPs, the solid circles represent the BCPs and the triangle is the ring critical point in $\rho(\mathbf{r})$. Crosses denote the positions of nuclei at the plane and open crosses represent the projections of out-of-plane nuclei. Contours are in steps of 2^m10^n e Å^{-5} ($m=1$–3; $n=-3$ to $+3$). Bond path, bcp (●) and rcp (△) include in (a), (c), (e).

Table 2
Topological properties associated with the BCPs of intramolecular interactions

Bond, BL (Å)	$d1$ (Å)	ρ_b (e Å^{-3})	$\nabla^2\rho_b$ (e Å^{-5})	H_b (a.u. Å^{-3})
H1–N1, 1.03	0.278	2.13	−33.55	−2.69
	0.292	1.88	−32.85	−2.59
	0.239	1.88	−22.11	−2.16
	0.175	1.88	−38.84	−2.58
N1–S1,	1.001	1.37	−5.98	−1.56
1.6880(7)	0.990	1.38	−5.22	−1.56
	0.891	1.42	−6.77	−1.34
	0.847	1.74	−5.25	−1.53
S1–S2,	1.023	0.98	−2.26	−0.52
2.0565(4)	1.027	1.00	−1.84	−0.52
	1.016	0.99	−1.08	−0.66
	0.983	0.88	−1.48	−0.56
S2–S3,	1.034	0.95	−1.92	−0.47
2.0708(5)	1.034	0.96	−1.61	−0.49
	1.012	0.94	−0.37	−0.61
	0.988	0.89	−1.00	−0.61
S3–S4,	1.028	0.98	−2.26	−0.51
2.0558(4)	1.028	0.99	−1.94	−0.52
	1.031	0.97	−0.34	−0.64
	1.054	1.14	−1.73	−0.75
S–S in S_8 2.050	1.024	0.98	−2.29	−0.51
S–S [19] 2.047	1.025	0.89	−2.57	
S–S [14], 2.023		1.09	−5.39	
		1.13	–0.59	
S–S [48], 2.006	1.00	1.08	−4.56	−0.67
	1.01	1.08	0.60	
S–S [12], 2.351	1.10	0.54	0.98	
	1.16	0.51	2.31	
S–S [12], 2.509	1.34	0.38	1.93	
	1.28	0.37	2.66	
S–S [12], 2.213	1.05	0.75	−0.88	
	1.08	0.70	2.75	

First line from DFT calculations of monomer, second line from PDFT calculation of crystal, third line from PDFT/MM, fourth line from KRMM. For other compounds: first line from calculation, second line from experiment.

originate at a saddle point and terminate at neighboring vertices define the edges, E, of the polyhedron. The set of trajectories that arise as a ring critical point define the faces, F. The numbers of each type of critical point satisfy the Euler's formula $V-E+F=2$. Based on the theoretical density map, the geometry of the atomic graph of nitrogen atom is a slightly distorted trigonal bipyramid (tbp). Three equatorial bonded CCs along N–S1, N–S1′ and H–N bonds and two axial non-bonded CCs ca. 0.4 Å above and beneath

Table 3
Atomic AIM charges

Atom	Monomer	PDFT	PDFT/MM	KRMM
H1	+0.40	+0.40	+0.53	+0.95
N1	−1.23	−1.18	−1.28	−1.49
S1	+0.47	+0.42	+0.31	+0.34
S2	−0.04	−0.02	+0.07	−0.04
S3	−0.01	−0.02	−0.05	−0.07
S4	+0.00	−0.01	+0.09	+0.09

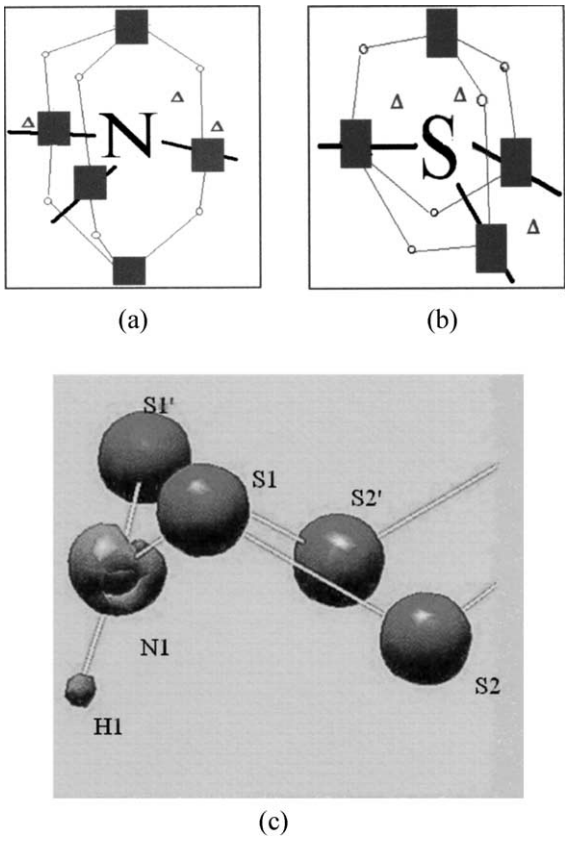

Fig. 4. Atomic graphs of (a) N1, (b) S4, ■ represents CC, ○ denotes edges, △ denotes faces, (c) 3D iso-value surface of Laplacian charge density maps ($\nabla^2\rho(\mathbf{r})=\pm31.0$ e Å^{-5}).

the core of N are found. Six edges and three faces are located as displayed in Fig. 4a. A corresponding 3D iso-value Laplacian surface around N1 is depicted in Fig. 4c. The geometry of the atomic graph of S atom is slightly distorted tetrahedron (T_d). There are four vertices: two non-bonded CCs and two bonded CCs, five edges and three faces as shown in Fig. 4b. The detail description of the polyhedron around N, S and H are given in supplementary material. The atomic graphs of S in S_7NH and S_8 are essentially the same.

3.5. Intermolecular interactions

Bifurcated hydrogen bonding. Hydrogen bonding is found between neighboring molecules in the crystal [10]. Due to the mirror symmetry, this H-bond has to be bifurcated. The existence of this bifurcated hydrogen bonding is reconfirmed by the topological properties analysis on charge density distributions. All ρ_b, $\nabla^2\rho_b$, H_b values of such H-bond listed in Table 4 are very small both in experiment and theory. The differences in BP and geometrical distance (BL) are noticeable, BL = 2.617 Å, BP = 2.880 Å (experiment), 2.715 Å (crystal), 2.713 Å (dimer). Therefore, the hydrogen bonds are slightly bent of course it could be due to the uncertainty of BP for such a weak interaction. The close to zero H_b value and positive

Table 4
Topological properties associated with BCPs for intermolecular interactions

Bond, BL (Å)	$d1$ (Å)	ρ_b (e Å^{-3})	$\nabla^2\rho_b$ (e Å^{-5})	G_b (kJ mol^{-1} Å^{-3})	H_b (kJ mol^{-1} Å^{-3})	BP (Å)	ΔE (kJ mol^{-1})
H(1)[a]···S(1),	0.873	0.10	0.90	156.4	9.7	2.713	−14.04
2.617(2)	0.904	0.10	0.84	149.0	6.0	2.715	
	1.047	0.12	1.02	187.3	0.9	2.620	
	1.066	0.09	0.59	110.9	−2.0	2.880	−8.4[b]
N(1)[c]···S(4),	1.619	0.06	0.61	94.5	18.0	3.364	−5.54
3.3645(3)	1.621	0.06	0.59	92.1	16.8	3.364	
	1.685	0.07	0.84	128.5	26.5	3.364	
	1.722	0.06	0.58	90.8	16.2	3.379	
S(2)···S(3)[d],	1.729	0.05	0.61	89.4	23.1	3.569	−3.14
3.5593(2)	1.838	0.06	0.59	92.1	16.8	3.569	
	1.825	0.06	0.56	88.4	15.0	3.566	
	1.795	0.05	0.62	90.6	23.8	3.569	
S(4)···S(3)[e],	1.841	0.04	0.53	75.1	22.7	3.673	−5.82
3.6477(3)	1.840	0.05	0.51	77.1	17.0	3.665	
	1.926	0.07	0.68	108.8	16.6	3.668	
	1.905	0.06	0.63	97.0	19.3	3.704	
S···S [19],	1.717	0.08	0.53	96.7	1.1		
3.426							
S···S [14],		0.04	0.44	64.0	17.1		
3.669							

First line from DFT calculations of dimer, second line from PDFT calculation of crystal, third line from PDFT/MM, fourth line from KRMM. For other compounds from calculation: first line from calculation, second line from experiment.

[a] $-1/2+X$, $1/2-Y$, $1/2-Z$.

[b] Calculated based on [41].

[c] X, Y, $-1+Z$.

[d] $-X$, $1-Y$, $-Z$.

[e] $-1/2+X$, $1/2-Y$, $-1/2-Z$.

value of $\nabla^2\rho_b$ indicate a closed-shell interaction of hydrogen bonding. The kinetic energy density G_b is 110.9 kJ mol^{-1} Å^{-3}. The binding interaction energy of this hydrogen bonding, ΔE, of −14.04 kJ mol^{-1}, is based on the dimeric model calculation taking account of the BSSE correction (7.31 kJ mol^{-1}). It appears a weak hydrogen bond in solid, which is very close to the H-bond found in HCN [48] on the accounts of ρ_b and ΔE values. Following the Abramov's expression and Espinosa's statistic survey on D_e vs d(O···H) [41], the experimental ΔE would be −8.4 kJ mol^{-1} (Table 4). For depicting this bifurcated hydrogen bonding, Fig. 5 shows the Laplacian charge density distribution at the S1H(1)S1′ plane including the bifurcated H-bond. It is clear both in experiment and theory that the non-bonded CC of S is directed toward the H atom, forming a directional Lewis acid–base pair.

N1···S(4) binding interactions. In addition to hydrogen bonding there are N···S and S···S intermolecular interactions in the solid. The N1 atom binds with the S4 of the neighboring moiety. The ρ_b values of N1···S(4) and S···S are close to those of the reported [20] values in S_4N_4 [ρ_b=0.085, 0.043 e Å^{-3}]. Based on the dimeric model, the BSSE corrected binding interaction energy of N1···S(4) interaction, ΔE, is −5.54 kJ mol^{-1}. The BP and BL values are the same at 3.364 Å. The non-bonded Laplacian CC of N1 is toward the secondary Laplacian charge depletion of S4. The typical Lewis acid–base directional interaction is shown in Fig. 6 as the Laplacian distributions at the H1N1S(4) plane.

S···S binding interactions. The S2 atom binds with the neighboring S(3) atom in pairs. The intermolecular S···S distances are slightly shorter than the sum of van der Waals radii. A BCP is located between the two atoms. Due to the symmetry exhibited in the crystal, this S···S interaction has to be in pairs shown in Fig. 7. The experimental ρ_b and $\nabla^2\rho_b$ values of this S···S binding interaction agree well with those in L-cystine [ρ_b=0.02–0.03 e Å^{-3} and $\nabla^2\rho_b$=0.53 e Å^{-5}] [19]. The binding interaction energies of S2···S(3) is −3.14 kJ mol^{-1}. Again, it can be visualized with one of the Laplacian vertices around S2 pointing towards the Laplacian face of S(3) of the neighboring moiety forming the S2···S(3) directional interaction. Fig. 7f gives a 3D isovalue surface of Laplacian for this interaction. The bonded CCs of sulfur atoms are not shown here for clarity. There is an other types of S···S interaction in the crystal, due to the mirror symmetry, the bifurcated S···S interactions are located between S4 and two S(3) atoms of neighboring moiety. The ρ_b, $\nabla^2\rho_b$ and H_b values are close to those of S2···S(3) interaction, so as the Laplacian distribution. The BSSE corrected binding interaction energy for each of the interaction, ΔE, is estimated as −5.82 kJ mol^{-1}. All these H···S, S···S, and N···S weak intermolecular interactions should be closed-shell interactions according to

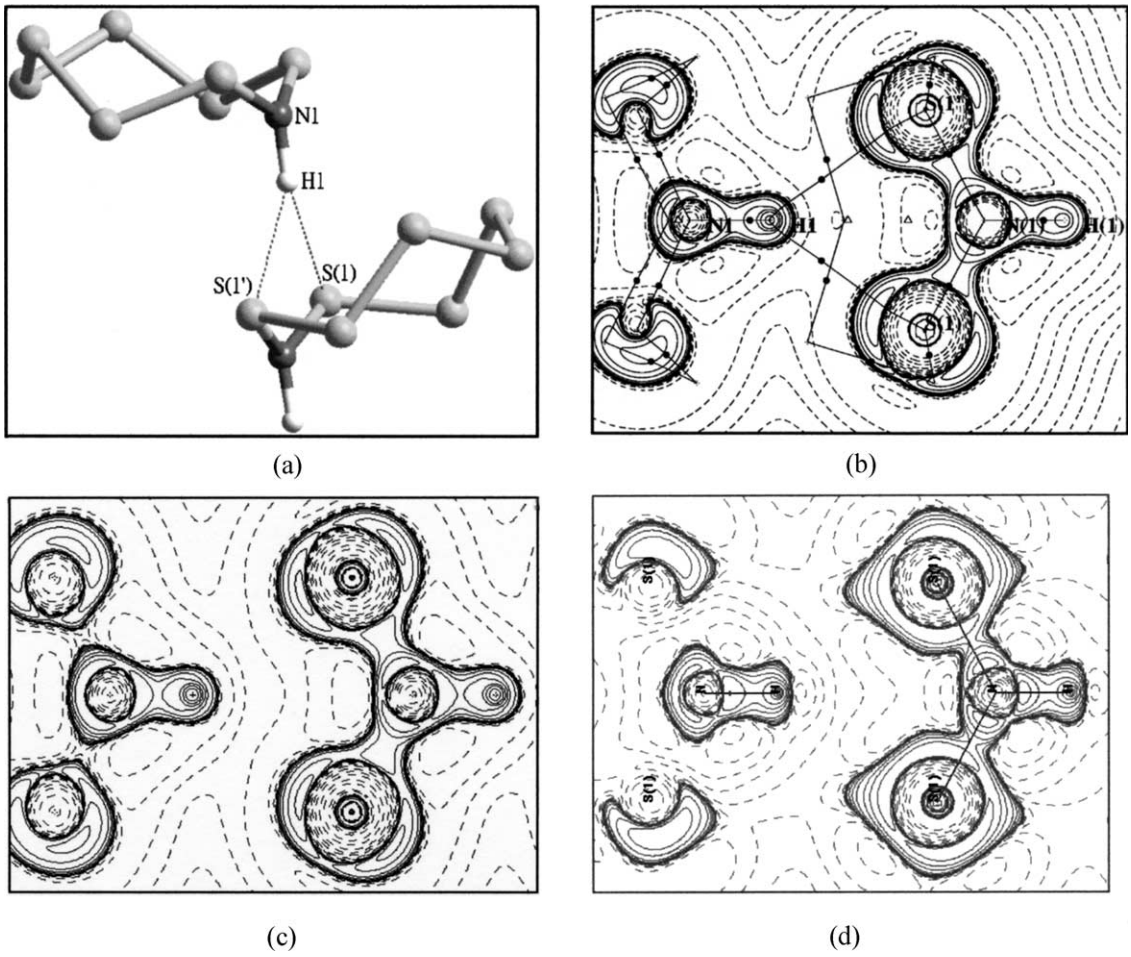

Fig. 5. The Laplacian distribution of bifurcated hydrogen bonded interactions at the projection of S1–H1–S1′ (a) the model of chosen dimer; (b) from the DFT calculation of this dimer; (c) from PDFT calculation of the crystal and (d) from the experiment (KRMM), contours are as in Fig. 3.

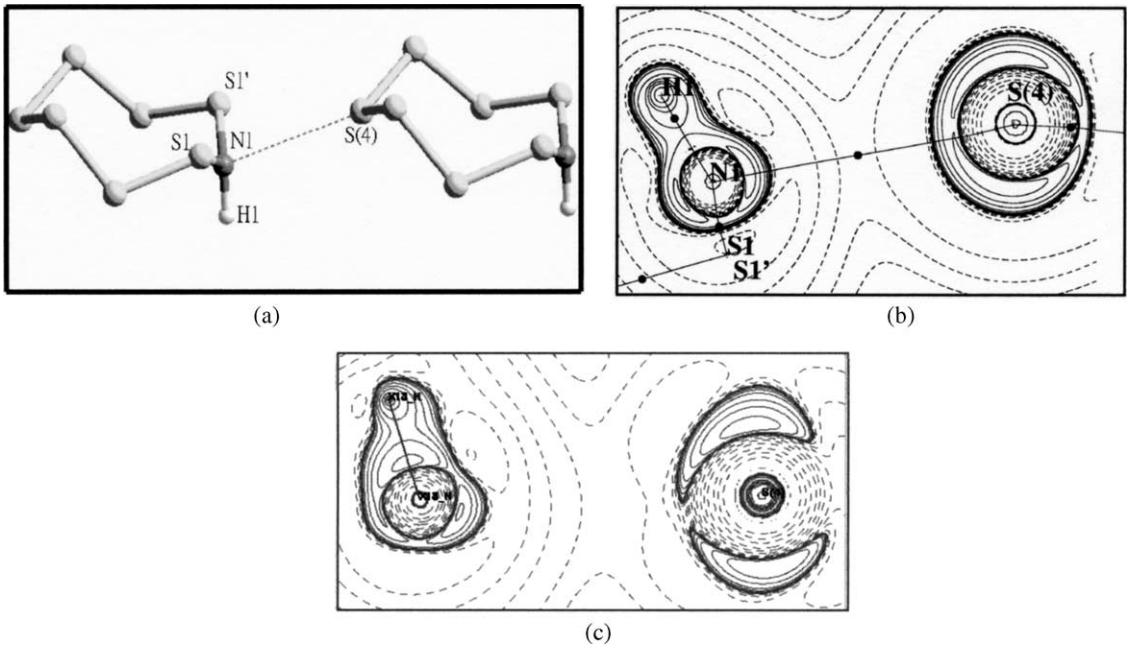

Fig. 6. The Laplacian distribution of N1⋯S(4) interactions at the projection of H1–N1–S4′, (a) the model of chosen dimer; (b) from the experiment (KRMM), contours and notations are as in Fig. 3.

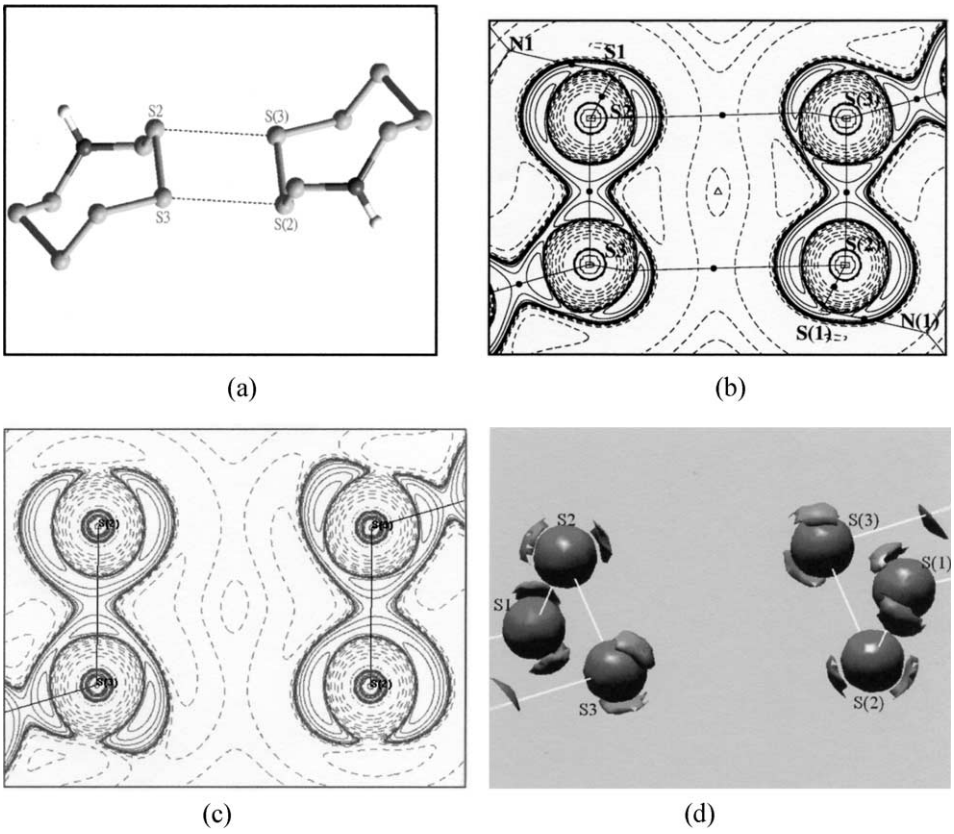

Fig. 7. The Laplacian distribution of S2···S(3) and S3···S(2) intermolecular interactions at the projection of S2–S3–S2′, (a)–(c) are defined as in Fig. 6, contours and notations are as in Fig. 3. The 3D iso-value surface of Laplacian ($\nabla^2\rho(\mathbf{r}) = -11.0$ e Å^{-5}) is shown in (d).

the topological analyses (see Table 4). The kinetic energy density, G_b, values at the BCPs of S···S, and N···S weak interactions are ca 14 kJ mol^{-1} a.u.$^{-3}$ volume, which is the same as those in L-cystine [19]. These interactions are similar to the van der Waals interaction as calculated in the Ar···HF and Ne···HF complexes [21]. Even for such a weak intermolecular interaction, the directional interaction between a Laplacian concentration and Laplacian depletion can be visualized and a quantitative description of a Lewis acid–base pair is provided. The low ρ_b values are consistent with the calculated low binding interaction energies. The order of the strength of these intermolecular interactions is N–H···S > N···S ≈ S···S.

4. Summary

The topological properties analyses of the charge density distributions have been dealt with the monomer, the chosen dimer and the crystal both by experiment and by theory (DFT and PDFT). The chemical aspects of the charge density distribution for intra and intermolecular interactions are described. The nature of the bifurcated hydrogen bonding and the existence of N···S, S···S weak interactions in solid state have been characterized as directional interactions. The directional interaction based on Laplacian topology provides a clear description of Lewis acid–base concept. It is a promising tool and an important advance to extend our understanding not only of molecular structure, but also of weak intermolecular interactions.

Acknowledgements

The authors thank the National Science Council of Republic of China for the financial support and are grateful to National Center for High-Performance Computing for the access of their computing facility and software packages.

Appendix. Supplementary Material

Supplementary data associated with this article can be found, in the online version, at 10.1016/j.jpcs.2004.08.007

References

[1] P. Coppens, Y.W. Yang, R.H. Blessing, W.F. Cooper, F.K. Larsen, J. Am. Chem. Soc. 99 (1977) 760–766.
[2] A. Kirfel, G. Will, Acta Crystallogr. B 36 (1980) 512–523.

[3] Y. Elerman, J.W. Bats, H. Fuess, Acta Crystallogr. C 39 (1983) 515–518.
[4] T.-H. Tang, R.F.W. Bader, P.J. MacDougall, Inorg. Chem. 24 (1985) 2047–2053.
[5] Y. Wang, M.J. Chen, C.H. Wu, Acta Crystallogr. B 44 (1988) 179–182.
[6] Y. Wang, J.H. Liao, Acta Crystallogr. B 45 (1989) 65–69.
[7] Y. Wang, S.Y. Wu, A.C. Cheng, Acta Crystallogr. B 46 (1990) 850–854.
[8] Y. Wang, S.K. Yeh, C.H. Wu, C.T. Pai, C.R. Lee, K.J. Lin, Acta Crystallogr. B 47 (1991) 298–303.
[9] S.K. Yeh, Y. Wang, Acta Crystallogr. B 48 (1992) 319–324.
[10] C.C. Wang, Y.-Y. Hong, C.-H. Ueng, Y. Wang, J. Chem. Soc. Dalton Trans. (1992); 3331–3336.
[11] K.J. Lin, Y. Wang, J. Phys. Chem. 97 (1993) 3176–3182.
[12] T.S. Hwang, Electron density distribution and bond characterizations on sulfur containing compounds and a nickel-complex, PhD Thesis, National Taiwan University, Taipei, Taiwan, ROC, 1996.
[13] A.S. Brown, V.H. Smith, J. Chem. Phys. 99 (1993) 1837–1839.
[14] K. McCormack, P.R. Mallinson, B.C. Webster, D.S. Yufit, J. Chem. Soc., Faraday Trans. 92 (1996) 1709–1716.
[15] R. Gleiter, R. Hoffman, Tetrahedron 24 (1968) 5899–5911.
[16] M.A. Ratner, J.R. Sabin, J. Am. Chem. Soc. 99 (1977) 3954–3960.
[17] C. Cohen-Addad, M.S. Lehman, P. Becker, L. Parkanyi, A. Kalman, J. Chem. Soc., Perkin Trans. 2 (1984) 191–196.
[18] (a) J.A. Dobado, H. Martinez-Garcia, J.M. Molina, M.R. Sundberg, J. Am. Chem. Soc. 120 (1998) 8461–8471;
(b) J.A. Dobado, H. Martinez-Garcia, J.M. Molina, M.R. Sundberg, J. Am. Chem. Soc. 121 (1999) 3156–3164.
[19] S. Dahaoui, V. Pichon-Pesme, J.A.K. Howard, C. Lecomte, J. Phys. Chem. A103 (1999) 6240–6250.
[20] W. Scherer, M. Spiegler, B. Pedersen, M. Tafiposky, W. Hieringer, B. Reinhard, A.J. Downs, G.S. McGrady, Chem. Commun. (2000); 635–635.
[21] R.F.W. Bader, Atoms in Molecules: A Quantum Theory, Clarendon Press, Oxford, 1990.
[22] (a) M.T. Carroll, C. Chang, R.F.W. Bader, Mol. Phys. 63 (1988) 387–405;
(b) T.-H. Tang, W.-J. Hu, D.-Y. Yan, Y.-P. Cui, J. Mol. Struct. (THEOCHEM) 207 (1990) 319–326;
(c) D.M. Whitefield, T.-H. Tang, J. Am. Chem. Soc. 115 (1993) 9648–9654;
(d) U. Koch, P.L.A. Popelier, J. Phys. Chem. 99 (1995) 9747–9754;
(e) T.-H. Tang, Y.-P. Cui, Can. J. Chem. 74 (1996) 1162–1170;
(f) P.L.A. Popelier, J. Phys. Chem. A102 (1998) 1873–1878;
(g) C.R. Lee, T.-H. Tang, L. Chen, Y. Wang, Chem. Eur. J. 9 (2003) 3112–3121.
[23] V.G. Tsirelson, P.F. Zou, T.-H. Tang, R.F.W. Bader, Acta Crystallogr. A 51 (1995) 143–153.
[24] R.G.A. Bone, R.F.W. Bader, J. Phys. Chem. 100 (1996) 10892–10911.
[25] (a) C.C. Wang, T.-H. Tang, Y. Wang, J. Phys. Chem. A104 (2000) 9566–9572;
(b) C.-R. Lee, C.C. Wang, K.-C. Chen, G.-H. Lee, Y. Wang, J. Phys. Chem. A103 (1999) 156–165;
(c) J.J. Lee, G.H. Lee, Y. Wang, Chem. Eur. J. 8 (2002) 1821–1832.
[26] (a) Y. Aray, R.F.W. Bader, Surf. Sci. 351 (1996) 233–249;
(b) Y. Aray, J. Rodriguez, D. Vega, J. Phys. Chem. B104 (2000) 5225–5231.
[27] Y. Aray, J. Rodriguez, D. Vega, E.N. Rodriguez-Arias, Angew. Chem. Int. Ed. 39 (2000) 3810–3813.
[28] (a) N.K. Hansen, P. Coppens. Acta Crystallogr., A34 (1978) 909–921
(b) P. Coppens, X-ray Charge Densities and Chemical Bonding, Oxford University Press, Oxford, 1997.
[29] T. Koritsanszky, S. Howard, T. Richter, Z. Su, P.R. Mallinson, N.K. Hansen, XD Computer Program Package for Multipole Refinement and Analysis of Electron Densities from X-ray Diffraction Data, Free University of Berlin, Germany, 1996.
[30] N–Hbond length ca 1.03 Å: c.f. F.H. Allen, Acta Crystallogr. B42 (1986) 515–522.
[31] A. Volkov, C. Gatti, Yu. Abramov, P. Coppens, Acta Crystallogr. A56 (2000) 252–258.
[32] M. Souhassou, R.H. Blessing, J. Appl. Crystallogr. 32 (1999) 210–217.
[33] M.J. Frisch, G.W. Trucks, H.B. Schlegel, G.E. Scuseria, M.A. Robb, J.R. Cheeseman, V.G. Zakrzewski, J.A. Montgomery R.E., Stratmann, J.C. Burant, S. Dapprich, J.M. Millam, A.D. Daniels, K.N. Kudin, M.C. Strain, O. Farkas, J. Tomasi, V. Barone, M. Cossi, R. Cammi, B. Mennucci, C. Pomelli, C. Adamo, S. Clifford, J. Ochterski, G.A. Petersson, P.Y. Ayala, Q. Cui, K. Morokuma, D.K. Malick, A.D. Rabuck, K. Raghavachari, J.B. Foresman, J. Cioslowski, J.V. Ortiz, B.B. Stefanov, G. Liu, A. Liashenko, P. Piskorz, I. Komaromi, R. Gomperts, R.L. Martin, D.J. Fox, T. Keith, M.A. Al-Laham, C.Y. Peng, A. Nanayakkara, C. Gonzalez, M. Challacombe, P.M.W. Gill, B.G. Johnson, W. Chen, M.W. Wong, J.L. Andres, M. Head-Gordon, E.S. Replogle, J.A. Pople, GAUSSIAN 98 (Revision A.7), Gaussian, Inc., Pittsburgh, PA, 1998.
[34] C. Lee, W. Yang, R.G. Parr, Phys. Rev. B37 (1988) 785–789.
[35] A.D. Becke, J. Chem. Phys. 98 (1993) 5648–5652.
[36] C. Møller, M.S. Plesset, Phys. Rev. 46 (1934) 618–622.
[37] S.F. Boys, F. Bernardi, Mol. Phys. 19 (1970) 553–566.
[38] V.R. Saunders, R. Dovesi, C. Roetti, M. Causà, N.M. Harrison, R. Orlando, C.M. Zicovich-Wilson, CRYSTAL 98 User's Manual, University of Torino, Italy, 1998.
[39] R.F.W. Bader, J. Phys. Chem. A102 (1998) 7314–7323.
[40] (a) R.F.W. Bader, T.-H. Tang, Y. Tal, F.W. Biegler-König, J. Am. Chem. Soc. 104 (1982) 946–952;
(b) R.F.W. Bader, T. Slee, D. Cremer, E. Kraka, J. Am. Chem. Soc. 105 (1983) 5061–5068;
(c) D. Cremer, E. Kraka, Croat. Chem. Acta 57 (1984) 1259–1281.
[41] (a) Y. Abramov, Acta Crystallogr. A53 (1997) 264–272;
(b) E. Espinosa, E. Molins, C. Lecomte, Chem. Phys. Lett. 285 (1998) 170–173.
[42] C.-R. Lee, L.Y. Tan, Y. Wang, J. Phys. Chem. Solids 62 (2001) 1613–1628.
[43] R.F.W. Bader, P.L.A. Popelier, C. Chang, J. Mol. Struct. (THEOCHEM) 255 (1992) 145–147.
[44] R.F.W. Bader, et al., AIMPAC: a Set of Programs for the Theory of Atoms in Molecules, McMaster University, Hamilton, Ont., Canada L8S 4M1, 1994.
[45] D.-C. Fang, T.-H. Tang,, AIM98PC, The Modified PC Version of AIMPAC, 1998.
[46] C. Gatti, TOPOND 98 User's Manual, CNR-CSRSRC, Milano, Italy, 1998.
[47] P. Macchi, B.B. Iversen, A. Sironi, B.C. Chakoumakos, F.K. Larsen, Angew. Chem. Int. Ed. 39 (2000) 2719–2722.
[48] J.A. Platts, S.T. Howard, J. Chem. Phys. 105 (1996) 4668–4674.
[49] A. Volkov, Y. Abramov, P. Coppens, C. Gatti, Acta Crystallogr. A 56 (2000) 332–339.
[50] A. Karpfen, P. Schuster, J. Petkov, H. Lisdika, J. Chem. Phys. 68 (1978) 3884–3890.
[51] (a) R.J. Gillespie, I. Hargittai, The VSEPR Model of Molecular Geometry, Allen and Bacon, Boston, 1991;
(b) R.F.W. Bader, R.J. Gillespie, P.J. MacDougall, J. Am. Chem. Soc., 110 (1998) 7234–7235;
(c) R.J. Gillespie, E.A. Robinson, Angew. Chem. Int. Ed., 35 (1996) 495–514.